Flow dynamics of vitreous humour during saccadic eye movements

Citation for published version:
Fonseca Da Silva, A, Pimenta, F, Alves, MA & Oliveira, MSN 2020, 'Flow dynamics of vitreous humour during saccadic eye movements', *Journal of the mechanical behavior of biomedical materials*, vol. 110, 103860. https://doi.org/10.1016/j.jmbbm.2020.103860

Digital Object Identifier (DOI):
10.1016/j.jmbbm.2020.103860

Link:
Link to publication record in Edinburgh Research Explorer

Document Version:
Peer reviewed version

Published In:
Journal of the mechanical behavior of biomedical materials

Flow dynamics of Vitreous Humour during saccadic eye movements

Andreia F. Silva[a,b,*], Francisco Pimenta[c], Manuel A. Alves[c], Mónica S.N. Oliveira[a]

[a] *James Weir Fluids Laboratory, Department of Mechanical and Aerospace Engineering, University of Strathclyde, Glasgow G1 1XJ, UK*

[b] *School of Physics and Astronomy, University of Edinburgh, King's Buildings, Mayfield Road, Edinburgh EH9 3JL, UK*

[c] *Departamento de Engenharia Química, CEFT, Faculdade de Engenharia, Universidade do Porto, 4200-465 Porto, Portugal*

Abstract

In this work, we reveal the flow dynamics of Vitreous Humour (VH) gel and liquid phases during saccadic movements of the eye, considering the biofluids viscoelastic character as well as realistic eye chamber geometry and taking into account the saccade profile. We quantify the differences in the flow dynamics of VH gel and liquid phases using viscoelastic rheological models that are able to model the VH shear rheology, considering different amplitudes of saccadic movements (10°, 20°, 30° and 40°). For this purpose, the computational fluid dynamics (CFD) open source software OpenFOAM® was used. The results portray a distinct flow behaviour for the VH gel and liquid phases, with inertial effects being more significant for the VH liquid phase. Moreover, the Wall Shear Stress (WSS) values produced by the VH gel phase are more than the double of those generated by the VH liquid phase. Results also show that for different amplitudes of eye movement both the velocity magnitude in the vitreous cavity and the shear stresses on the cavity walls rise with increasing saccadic movement displacement.

*Corresponding author
Email address: andreia.silva@ed.ac.uk (Andreia F. Silva)

Preprint submitted to Journal of the Mechanical Behavior of Biomedical Materials May 13, 2020

Keywords: Vitreous Humour, viscoelastic fluids, flow dynamics, saccadic movements

1. Introduction

The human eye has one of the fastest muscles in the body, being able to produce rotations of 40 degrees in approximately 100 ms [1]. In the different situations of daily life, the eyes are able to produce different, voluntary or involuntary, movements. Saccadic eye movements are the most common movements of the eye. They are very quick ballistic movements produced by both eyes simultaneously and in the same direction when fixating an object [2, 3, 4]. In fact, the eyes are never completely at rest, because they are constantly producing saccades. How these movements affect the dynamics of the eye's fluids is not yet fully understood.

The majority of the eyeball, more specifically the space between the lens and the retina, is filled with Vitreous Humour (VH) fluid, a transparent gelatinous avascular structure [5, 6, 7, 8, 9], which exhibit non-Newtonian rheological behaviour [9]. The major constituents of the biofluid are long collagen fibrils suspended in patterns of hyaluronic acid or hyaluronan (HA) molecules and others glycosaminoglycans (GAGs), which surround and stabilise water molecules. This fluid is only produced during the embryonic stage and is not replenished throughout the entire life of a person [10]. It is known that as a consequence of ageing and/or some diseases the VH becomes progressively liquefied [11], with the corresponding rheological properties varying during lifetime. Many of the eye's diseases are directly or indirectly associated with the morphological changes of this biofluid with age, and consequent changes in its flow behaviour and performance [12, 13].

Over the years, several studies regarding VH flow behaviour have been performed using numerical, analytical, or experimental approaches. Table 1 presents a summary of the key points of those studies. In the late 1990's, David *et al.* [14]

presented both analytical and numerical solutions for a time-dependent motion of the VH during saccadic motion of the eye. The authors studied analytically the motion of a viscoelastic fluid, and also tested numerically the case of a Newtonian fluid. The vitreous cavity was simulated as a perfect sphere and a sinusoidal function was used to represent the saccadic movements. In 2005, Repetto *et al.* [15] presented an experimental study of the VH motion induced by saccadic eye movements (see the key points of the study in Table 1). The authors considered VH as a Newtonian fluid, and the eye as a perfect sphere. Despite the simplifications assumed, both David *et al.* [14] and Repetto *et al.* [15] studies were critical starting points to understand the flow patterns during saccadic movements. In the following years, Repetto *et al.* [12, 16] and Stocchino *et al.* [13, 17] performed analytical and experimental studies, respectively, of the dynamics of the VH induced by saccadic movements. The eye models were created based on the same assumptions as in [15], but an improved non-spherical shape was considered to resemble the real vitreous chamber. Their results showed that the non-spherical shape of the cavity generates flow fields and stresses on the boundary that are significantly different from those generated in the case of motion within a sphere, with vortices forming in the area of the lenses indentation, which the authors believed might play a role in the generation of retinal detachments. Abouali *et al.* [18] analysed saccadic movements with a range of amplitudes from 10 to 50°. Their eye model had the size of the real human eye, with a radius of 12 mm and different degrees of indentation resembling the lenses shape in the anterior part of the eye. All the studies mentioned so far helped to increase our understanding of the flow dynamics of the biofluid during saccadic eye movements, and/or provided insights to understand the importance of considering the lenses indentation. However, all of those works were performed using Newtonian fluids, while it is known that both VH phases exhibit viscoelastic rheological behaviour [9] and that their rheology is closely related to its functionality in the eye. Therefore, assuming that the biofluid has a Newtonian rheology is an oversimplification that can lead to significant differences in terms of the predicted flow behaviour during saccadic eye movements.

The first studies about eye movements considering fluids with viscoelastic properties were published in 2011 [19, 20]. However, both studies considered the eye as a sphere. The study of Meskaukas *et al.* [20] showed that the maximum velocity inside the eye cavity can be twice the maximum wall velocity, and that resonance effects related with the viscoelasticity of the fluids generate larger wall shear stresses, and could be relevant for the occurrence of retinal detachment. Those results were later corroborated by Isakova *et al.* [21], who predicted the same trend using an analytical approach, and also by Bonfiglio *et al.* [22] who also obtained similar results based on an experimental study. Modarreszadeh and Abouali [23] focused on providing a reliable numerical procedure for the study of VH as a viscoelastic substance and under oscillatory movements. The open-source software OpenFOAM® was used and the viscoelastic solver developed by Favero *et al.* [24] was adapted to handle dynamic meshes. As their focus was to provide a reliable numerical tool, their paper presents mostly solver validations, and only preliminary results of the VH behaviour, considering a Giesekus model for the VH gel phase and a Newtonian liquefied phase under sinusoidal movement with frequency of 10 rad/s and amplitude of 3%, were presented.

In summary, there is a body of research work on the flow behaviour of vitreous humour. However, most of the studies rely on a variety of simplifications (e.g. simplified eye geometry, assumption of VH as a Newtonian fluid, considering sinusoidal movements) that may lead to significant differences in the flow behaviour when compared with the real VH in the eye. Additionally, to the best of our knowledge, there are no numerical studies that consider the viscoelastic behaviour of the VH liquid phase, as it is usually simulated as a Newtonian fluid [25, 19, 23].

The aim of this study is the numerical investigation of the flow behaviour of VH using adequate viscoelastic rheological models that are able to model the VH behaviour, using a geometry that is a better approximation of the vitreous humour chamber and real saccade profiles, to obtain a better insight about the flow dynamics of VH during saccadic movements. The remainder of the paper is organised as follows: the next section presents the numerical methodology used and the solver validations performed; the results are then presented and discussed; finally, the main conclusions are summarised in the last section.

Table 1: Summary of relevant numerical, analytical and experimental studies performed regarding the flow dynamics of VH.

Reference	Type	Geometry	Fluid rheology	Movement
David *et al.* 1988 [14]	Analytical and CFD	Sphere	Newtonian and viscoelastic	Sinusoidal
Repetto *et al.* 2005 [15]	Experimental	Sphere ($R = 40.8$ mm)	Newtonian	Saccades
Repetto *et al.* 2006 [12]	Analytical	Weakly deformed sphere	Newtonian	Saccades
Stocchino *et al.* 2007 [13]	Experimental	Weakly deformed sphere ($R = 40.8$ mm)	Newtonian	Sinusoidal
Repetto *et al.* 2010 [16]	Analytical	Weakly deformed sphere	Newtonian	Sinusoidal
Stocchino *et al.* 2010 [17]	Experimental	Weakly deformed spheres ($R = 40.8$ mm)	Newtonian	Sinusoidal
Repetto *et al.* 2011 [19]	CFD (Comsol Multiphysics®)	2D sphere ($R = 12$ mm)	Newtonian and viscoelastic model based on data from [7, 26]	Saccades
Meskauskas *et al.* 2011 [20]	CFD	Sphere	Newtonian and viscoelastic models based on data from [7, 26, 27]	Sinusoidal
Balachandran and Barocas 2011 [25]	CFD	Simplified eye geometry	Newtonian	Sinusoidal
Meskauskas *et al.* 2012 [28]	CFD	Sphere and different ellipsoids with an indentation	Newtonian and viscoelastic models based on data from [7, 26, 27]	Sinusoidal
Abouali *et al.* 2012 [18]	CFD (Fluent®)	Simplified eye geometry ($R = 12$ mm)	Newtonian	Saccades
Isakova *et al.* 2014 [21]	Analytical	Sphere	Newtonian and viscoelastic model based on data from [26]	Sinusoidal
Modarreszadeh and Abouali 2014 [23]	CFD (OpenFOAM®)	Simplified eye geometry ($R = 12$ mm)	Viscoelastic model based on data from [7]	Sinusoidal
Bonfiglio *et al.* 2015 [22]	Experimental	Sphere ($R = 12.5$ mm)	Viscoelastic model	Saccaddes
Natali *et al.* 2018 [29]	CFD	2D planar model	Newtonian	Saccaddes

2. Methodology

2.1. Eye model

The eye geometry used in the simulations was based on the real eye shape and size of an adult Human eye [30]. According to *Encyclopaedia Britannica Macropedia: Sensory Reception* [31], the dimensions of the eye are reasonably constant, with a variation of one or two millimetres between individuals, and with a vertical diameter of about 24 mm. The geometry was drawn with the 3D CAD design software SolidWorks® v.15 and the dimensions considered are shown in Fig. 1.

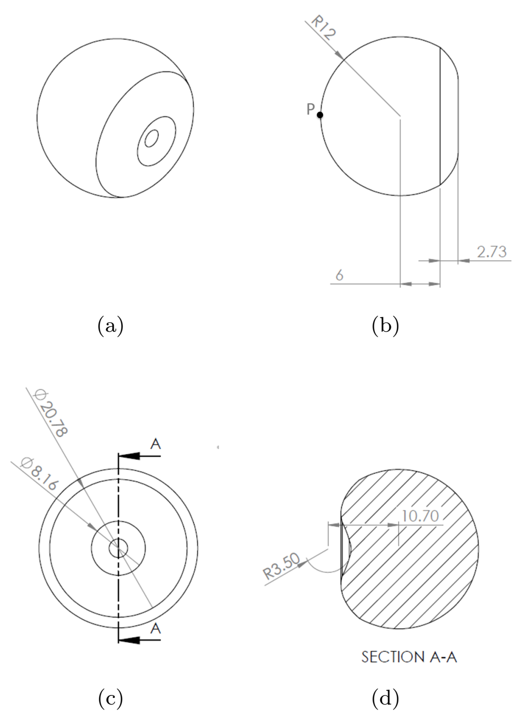

Figure 1: Computational model of the vitreous cavity: (a) 3D view; (b) side view; (c) front view; (d) midplane view based on section A-A presented in (c). All the dimensions are in millimetres.

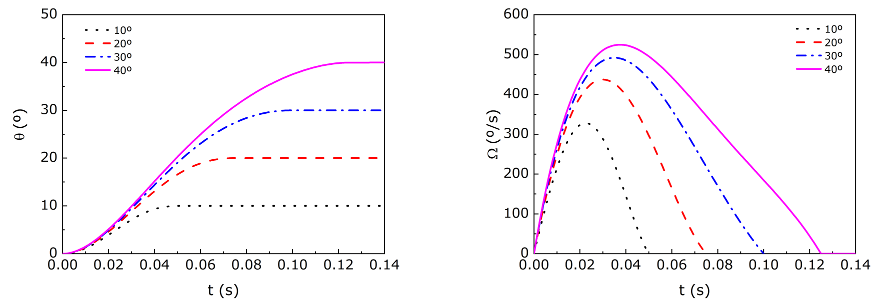

(a) (b)

Figure 2: (a) Angular displacement and (b) angular velocity of the saccadic eye movements under study.

2.2. Saccadic Movements

Saccadic movements are defined based on the saccade amplitude A, the saccade duration t_D, the peak angular velocity v_p and the acceleration time t_p. The fifth order polynomial equation presented by Repetto *et al.* [15], based in the experimental measurements from Becker [32], was used in this work to define the saccadic movements, and detailed information can be found in the supplementary material. The angular displacements under study are between 10° and 40°. The saccadic movement profiles, as well as the angular velocities related with each degree of displacement, are shown in Fig.2. The values of the saccade duration t_D and the acceleration time t_p for each degree of displacement are presented in Table 2.

Table 2: Values of the saccade duration t_D and the acceleration time t_p for each degree of displacement under study.

	Angular displacement (°)			
	10	20	30	40
t_p (s)	0.0225	0.03	0.035	0.0375
t_D (s)	0.05	0.075	0.1	0.1250

2.3. Constitutive models

In this investigation, the experimental rheological data measured in our previous work [9] was used for the selection of viscoelastic model parameters. Those experiments were performed using VH collected from New Zealand white rabbit specimen, which previous studies have shown to be a good pharmacokinetic model of human VH [33, 34]. The Giesekus model was used to fit the rheological behaviour of both the VH liquid and gel phases. This model was originally developed to describe the nonlinear response of polymeric solutions [35]. However, it has been proven suitable for gel-like solutions and it has subsequently been used in several studies to model their rheological behaviour [36, 37, 38, 39]. Due to the complex characteristics of the VH phases, several modes were required to reproduce the fluids behaviour: a 3-mode Giesekus model was able to accurately capture the experimental VH gel phase rheological data, while a 4-mode Giesekus model was used to fit the VH liquid phase rheological behaviour.

For the multimode Giesekus model, the shear viscosity is given by [40]

$$\eta(\dot{\gamma}) = \eta_s + \sum_k \frac{\eta_{p,k}(1-f_k)^2}{1+(1-2\alpha_k)f_k} \tag{1}$$

where the function f_k of mode k is given by

$$f_k = \frac{1-X_k}{1+(1-2\alpha_k)X_k} \quad \text{with} \quad X_k^2 = \frac{\sqrt{1+16\alpha_k(1-\alpha_k)(\lambda_k\dot{\gamma})^2}-1}{8\alpha_k(1-\alpha_k)(\lambda_k\dot{\gamma})^2} \tag{2}$$

The storage and loss moduli in SAOS are given by

$$G' = \sum_k \frac{\eta_{p,k}\lambda_k\omega^2}{1+(\lambda_k\omega)^2} \tag{3}$$

$$G'' = \eta_s\omega + \sum_k \frac{\eta_{p,k}\omega}{1+(\lambda_k\omega)^2} \tag{4}$$

where k is the mode index, varying from one to the number of modes used in the model, η_s and $\eta_{p,k}$ are the solvent and polymer viscosities of mode k respectively,

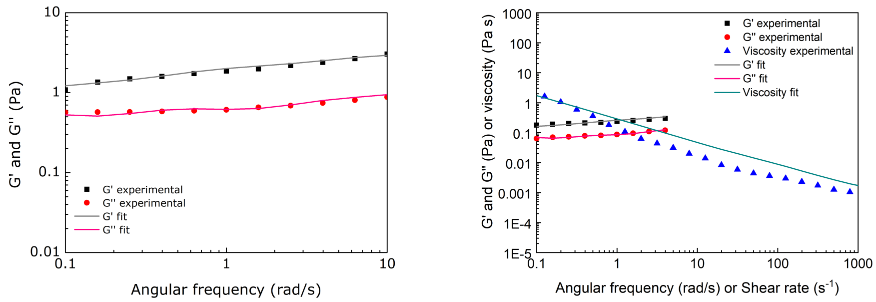

(a) (b)

Figure 3: Average storage and loss moduli as function of angular frequency, and shear viscosity as function of shear rate at $T = 37$ °C for (a) the gel phase of VH and the fit with a 3-mode Giesekus model, and (b) liquid phase of VH and the fit with a 4-mode Giesekus model. The experimental data is taken from [9].

λ_k is the relaxation time of mode k, ω is the angular frequency and α_k is the nonlinear parameter of mode k that is related with the anisotropy of the drag between the flow and the polymer segments [41]. Fig. 3 shows the experimental VH data and the data fit with the multimode Giesekus model for both the gel and liquid phases. Note that, for the liquid phase, G' is higher than the G'' for the range of frequencies presented, which is considered a gel-like behaviour. However, we refer to it as liquid phase for consistency with previous works [9]. The coefficients for each mode of the model are presented in Table 3. The density considered for both phases was 1006 kg/m^3 [11].

2.4. Numerical method

The open-source finite-volume code OpenFOAM® version 2.2.2 was used to solve the governing equations with the no-slip boundary condition applied in the whole eye surface, in a Cartesian coordinate system. A second-order implicit backward scheme was used to discretise the time-derivatives. To ensure the velocity-pressure coupling in a segregated way, the semi-implicit method for pressure-linked equations-Consistent (SIMPLEC) algorithm was selected. The

Table 3: Giesekus model parameters used to fit the rheological data of VH gel and liquid phases.

			Gel phase		
	mode 1	mode 2	mode 3		
λ_k (s)	35	2	0.2		
$\eta_{p,k}$ (Pa s)	45	1.7	0.2		
η_s (Pa s)				0.05	
α_k	0.5	0.5	0.5		
			Liquid phase		
	mode 1	mode 2	mode 3	mode 4	
λ_k (s)	35	2	0.2	0.01	
$\eta_{p,k}$ (Pa s)	6	0.2	0.035	0.006	
η_s (Pa s)					0.0007
α_k	0.5	0.5	0.5	0.5	

convective terms of the governing equations were discretized with the Convergent and Universally Bounded Interpolation Scheme for the Treatment of Advection (CUBISTA) [42], for both the momentum and constitutive equations. A zero pressure gradient normal to the walls was assumed. The log-conformation tensor reformulation was used to solve the constitutive equation, which is known to increase numerical stability [43, 44, 45].

2.5. Governing equations

For the cases under study, the whole eye model is moving as a solid body, with a prescribed motion, guaranteeing that the mesh does not suffer any topological change. In order to include the effect of the dynamic mesh, the convective terms in the governing equations needed to be corrected with the grid velocity. In this moving mesh framework, the continuity equation for an incompressible fluid can be written as

$$\nabla \cdot \mathbf{u} = 0 \tag{5}$$

where $\mathbf{u}$ is the velocity vector with components u_x, u_y and u_z in the x, y and z cartesian directions, respectively.

The Cauchy momentum equation can be written as

$$\rho\left[\frac{\partial \mathbf{u}}{\partial t} + \nabla \cdot \mathbf{u}(\mathbf{u} - \mathbf{u}_g)\right] = -\nabla p + \nabla \cdot \boldsymbol{\tau} + \rho \mathbf{g} \tag{6}$$

where ρ is the fluid density, p the pressure, t represents time, $\mathbf{u}_g$ refers to the velocity at which the grid is moving and $\mathbf{g}$ is the acceleration of gravity.

The space conservation law (SCL) needs to be satisfied to ensure mass conservation,

$$\frac{\mathrm{d}}{\mathrm{d}t}\int_V \mathrm{d}V - \int_S \mathbf{u}_g \cdot \mathbf{n}\mathrm{d}S = 0 \tag{7}$$

where V and S represent the volume and surface of the grid.

In order to solve the momentum equation, the extra-stress tensor $\boldsymbol{\tau}$ constitutive law has to be calculated. For viscoelastic fluids, the flow history is important, due to the memory of the fluid, and the total extra-stress tensor was split in a polymeric contribution $\boldsymbol{\tau}_p$ and a solvent contribution $\boldsymbol{\tau}_s$: $\boldsymbol{\tau} = \boldsymbol{\tau}_s + \boldsymbol{\tau}_p$. The Newtonian solvent contribution is given by

$$\boldsymbol{\tau}_s = \eta_s(\nabla \mathbf{u} + \nabla \mathbf{u}^{\mathrm{T}}) \tag{8}$$

while the the viscoelastic extra-stress $\boldsymbol{\tau}_p$ is computed based on the Giesekus equation, which for mode k is given by

$$\boldsymbol{\tau}_{p,k} + \lambda_k \overset{\triangledown}{\boldsymbol{\tau}}_{p,k} + \alpha_k \frac{\lambda_k}{\eta_{p,k}}(\boldsymbol{\tau}_{p,k}\boldsymbol{\tau}_{p,k}) = \eta_{p,k}(\nabla \mathbf{u} + \nabla \mathbf{u}^{\mathrm{T}}) \tag{9}$$

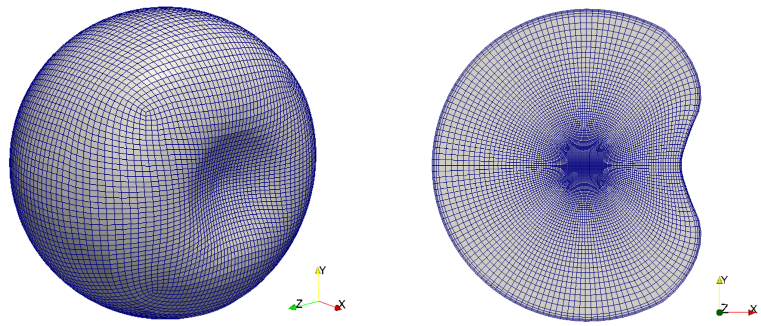

(a) (b)

Figure 4: Computational mesh used: (a) surface mesh; (b) cut of plane $z = 0$.

where η_s and $\eta_{p,k}$ are the solvent and the polymer viscosity of mode k contributions, respectively, λ_k is the relaxation time of mode k, and $\overset{\triangledown}{\boldsymbol{\tau}}_{p,k}$ is the upper-convective time derivative of $\boldsymbol{\tau}_{p,k}$, defined as $\overset{\triangledown}{\boldsymbol{\tau}}_{p,k} = \frac{\partial \boldsymbol{\tau}_{p,k}}{\partial t} + \mathbf{u} \cdot \nabla \boldsymbol{\tau}_{p,k} - \boldsymbol{\tau}_{p,k} \cdot \nabla \mathbf{u} - \nabla \mathbf{u}^{\mathrm{T}} \cdot \boldsymbol{\tau}_{p,k}$ [45].

2.6. Computational Mesh

To ensure accuracy of the CFD results, different levels of mesh refinement and different time steps were tested. The geometry was split in seven different blocks: a cube in the middle and six blocks around the central cube that meet the surface of the eye geometry. Meshes with 20, 40 and 80 cells per block and in each direction, with an additional refinement in the cell adjacent to the wall (area with higher gradients) were tested. The velocity profiles, along the vitreous cavity, at different times of the saccadic movement were compared and no significant differences were found between the results obtained with the meshes with 40 and 80 cells per block (see supplementary material), therefore the mesh with 40 cells in each direction was chosen (see Fig. 4). The origin of the coordinates system is in the centre of the cube in the middle of the geometry. All the cells are hexahedric and the total number of cells was 476 800 for the mesh used.

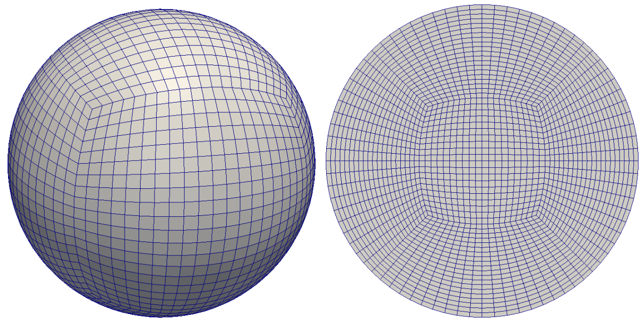

(a) (b)

Figure 5: Computational mesh used in the validation case of a sphere filled with a Newtonian fluid: (a) surface mesh; (b) mesh in the plane $z = 0$.

Two different time steps were tested, $\Delta t = 10^{-4}$ s and 10^{-5} s. Since no meaningful differences in the velocity profiles between these two time steps were observed, the time step $\Delta t = 10^{-4}$ s was chosen in all the remaining simulations.

2.7. Solver validation

2.7.1. Case 1: Sphere filled with a Newtonian fluid

David *et al.* [14] presented an analytical solution for Newtonian fluid motion of a sphere during oscillatory and saccadic movements. That model was used by Repetto *et al.* [15] and Abouali *et al.* [18] to validate their setups. Both used a spherical cavity with a radius of 40.8 mm, filled with glycerol. In this study, the same geometry, fluid and saccadic movement profile were chosen for validation: a saccadic movement with an amplitude $A = 40°$ and a period $t_D = 0.247$ s was applied to a Newtonian fluid with a kinematic viscosity of 8.19x10^{-4} m^2/s and a density of 1260 kg/m^3. The mesh used in this test is shown in Fig. 5, and consists of 56 000 cells split in 7 blocks.

The good agreement between the velocity magnitude profiles obtained and the theoretical profiles are shown in Fig. 6.

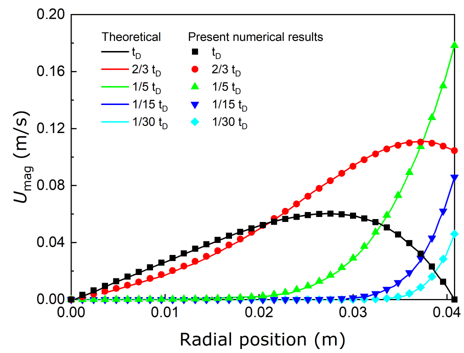

Figure 6: Comparison between theoretical (from [14, 15, 18]) and numerical velocity magnitude U_{mag} obtained in the present work for a saccadic movement with $A = 40°$ and duration $t_D = 0.247$ s.

2.7.2. Case 2: Sloshing cylinder filled with a viscoelastic fluid

In order to validate the numerical procedure for the flow dynamics of VH driven by saccadic movements, Modarreszadeh and Abouali [23] studied different geometries when subjected to sinusoidal oscillations. Different rheological models were tested in order to validate the methodology proposed for linear and non-linear regimes. A simulation with a 2D cylinder with a radius of $R = 0.012$ m, oscillating with amplitudes $A = 20°$ and with a constant angular velocity of $\omega = 10$ rad/s, corresponding to a period $t_D = 0.6283$ s, was performed in this work and compared with the results presented by Modarreszadeh and Abouali [23]. The VH was modeled with a 2-mode Giesekus model (see [23]), based on the rheological characteristics presented by [7], and a density $\rho = 1000$ kg/m^3 was used.

The 2D mesh used in this test is shown in Fig. 7 and consists of 11 200 cells. The results presented here were taken after 200 oscillation cycles, after the flow field reached the periodic state: after $n = 200$ cycles, $t_{t_D} = nt_D = 125.6640$ s, $t_{0.175t_D} = nt_D + 0.175t_D = 125.7740$ s, and $t_{0.25t_D} = nt_D + 0.25t_D = 125.8211$ s. The results of the tangential velocity profiles for the midline ($y = 0$) of the cylinder

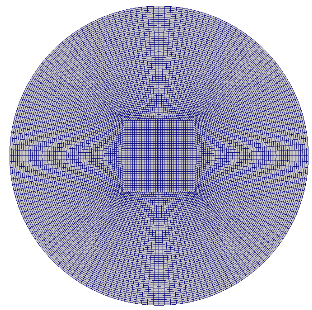

Figure 7: Computational mesh used in the validation with a 2D cylinder filled with a viscoelastic fluid modelled with a 2-mode Giesekus model.

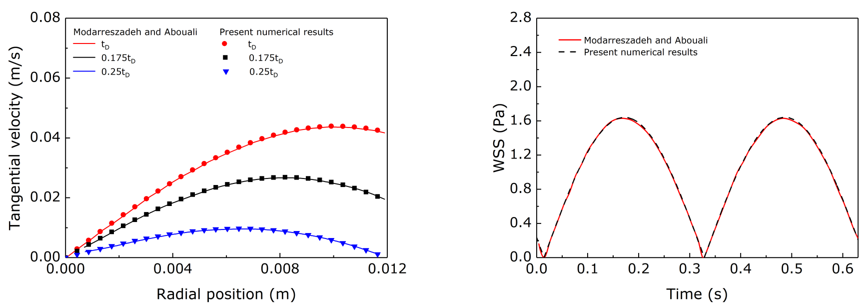

(a)

(b)

Figure 8: Comparison of (a) the tangential velocity profile and (b) the average wall shear stress magnitude profile obtained in this work and the results of Modarreszadeh and Abouali [23] for a 2D cylinder oscillating with an amplitude of $A = 20°$, and a constant angular velocity of $\omega = 10$ rad/s.

oscillating with amplitudes $A = 20°$ for the three different times mentioned above and the average WSS magnitude over an entire oscillating cycle are presented in Fig. 8.

The tangential velocity profiles obtained in this work show a good agreement with those obtained by Modarreszadeh and Abouali [23]. The average WSS magnitude in the wall of the 2D cylinder obtained in this work also shows the same profiles as in [23], with a maximum difference of about 0.8%.

3. Results and discussion

This section analyses the differences in the velocity magnitude and wall shear stress (WSS) of both VH phases, when subjected to different saccadic movement amplitudes, $A = 10$, 20, 30 and 40°.

3.1. Velocity field

The velocity contours in the midplane $z = 0$, of VH gel and VH liquid phase when the vitreous cavity is subjected to different degrees of movement, A, are presented in Fig. 9 and Fig. 10, respectively. The vitreous cavity rotates anti-clockwise around the z-axis. With the increase of the saccadic movement amplitude, A, the angular velocity applied in the vitreous cavity walls also increases (see Fig. 2) and, consequently, the velocities reached in the vitreous cavity increase. The momentum diffusion across the vitreous cavity also increases, and the more considerable differences between different degrees of movement can be found in the VH gel phase (see Fig. 9): for times $t = t_D$ and $t = 2t_D$, the portion of VH gel that exhibits very little deformation (in the centre of the cavity) decreases significantly with the increase of the saccadic amplitude, A, which is due to the higher elastic effects (higher Weissenberg number) observed at higher amplitudes, causing an increase of the fluid memory effects. VH gel phase is a network composed of collagen and HA molecules, and when subjected to deformation the molecules adjust their conformation. With time, this rearrangement will eventually cause degradation of the collagen molecules for higher deformations, which can lead to the appearance of VH liquid phase.

The VH liquid phase has a lower viscosity compared to the VH gel phase, which means that the diffusive time scale ($t_{diff} = \frac{\rho D^2}{\eta}$) is higher and for the initial times, $t = 0.1t_D$ and $t = t_p$, the velocity gradients occur primarily close to the walls (see Fig. 10). However, for $t \geq t_D$ the flow pattern changes significantly: for $t = 2t_D$ and an amplitude of 40° the fluid velocity magnitude reaches a

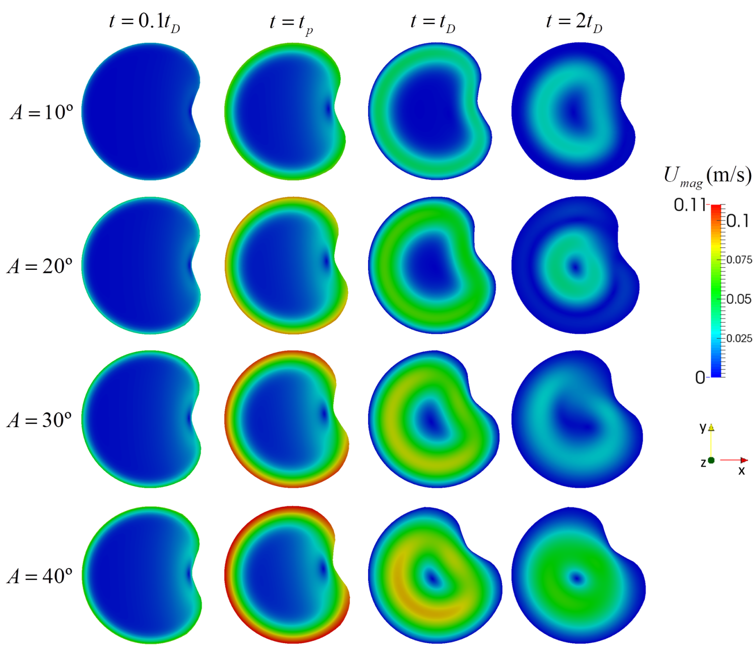

Figure 9: Velocity magnitude contours on plane $z = 0$ for saccadic movements with amplitudes $A = 10°$, $20°$, $30°$ and $40°$, at times $t = 0.1t_D$, $t = t_p$, $t = t_D$ and $t = 2t_D$, for VH gel phase.

maximum value around 0.06 m/s, which is more than half of the maximum velocity reached at the walls at $t = t_p$.

It is possible to observe that for times $t = 0.1t_D$ and $t = t_p$, right behind the lens indentation, a region where the velocity magnitude is close to zero (in fact there is a recirculation of fluid in that area) is formed for both VH gel and liquid phase, being more pronounced in the gel phase. The lens indentation significantly changes the flow patterns in the area behind it. Therefore, it is important to use a geometry that replicates the vitreous chamber geometry as closely as possible to avoid misleading results.

The analysis of different z-planes (not presented here) parallel to the one represented in Fig. 9 and Fig. 10 showed that in general, for the fluids under study, the velocity profiles follow similar trends to those observed in the central plane.

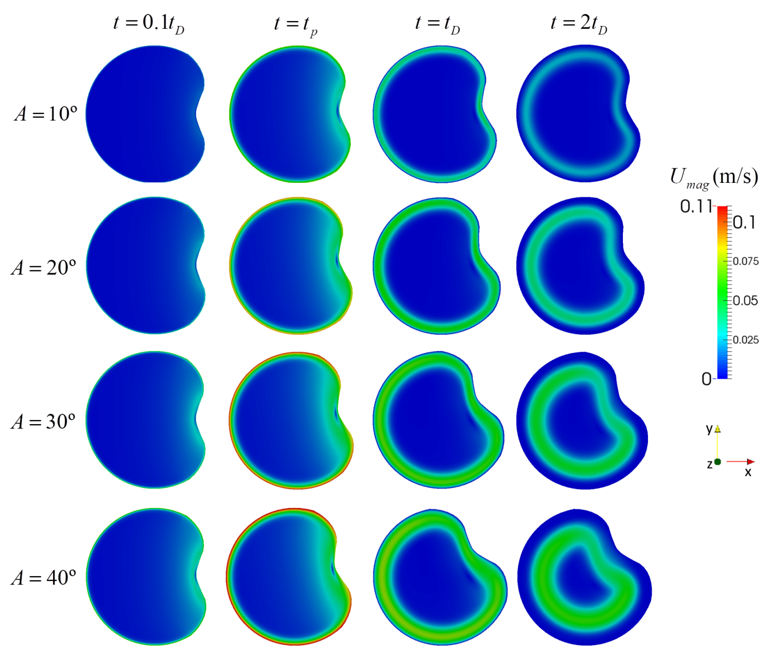

Figure 10: Velocity magnitude contours on plane $z = 0$ for saccadic movements with amplitudes $A = 10^{\circ}$, 20°, 30° and 40°, at times $t = 0.1t_D$, $t = t_p$, $t = t_D$ and $t = 2t_D$, for VH liquid phase.

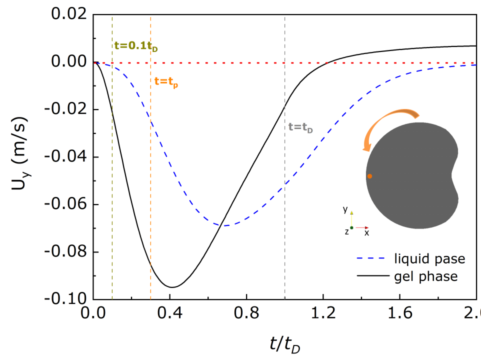

Figure 11: Velocity component U_y over time for VH liquid and gel phases at the point with coordinates (-11,0,0) mm during a saccadic movement with amplitude $A = 40°$.

For $t > t_D$ there are considerable velocity gradients inside the vitreous cavity. It was expected that due to memory effects of the viscoelastic fluids, soon after the vitreous cavity stops moving, the VH would flow back in the opposite direction of the imposed movement (recoil). The velocity component U_y over time at the point with coordinates (-11,0,0) mm is presented in Fig. 11. There is no change in the sign of the velocity U_y for the VH liquid phase, which means the flow keeps its original direction, indicative of lack of significant memory effects (inertial effects are stronger than elastic effects). For the VH gel phase, the sign of the velocity U_y changes at $t/t_D = 1.24$, showing a memory effect as the direction of the flow is reverted (elastic effects are dominant).

3.2. Wall shear stress

The wall shear stress on point P, $\mathrm{WSS_p}$ (see Fig. 1b), over time, and of the WSS contours for VH gel phase are presented in Fig. 12 and Fig. 13, respectively, for different amplitudes. Point P is located in the posterior position of the vitreous chamber (point with coordinates (-12,0,0) mm) and corresponds to a position close to the centre of the macula. The $\mathrm{WSS_p}$ for different amplitudes follows the same trend: with the increase of the imposed amplitude, the first peak of the $\mathrm{WSS_p}$ occurs earlier and the corresponding values are higher (the $\mathrm{WSS_p}$ peak

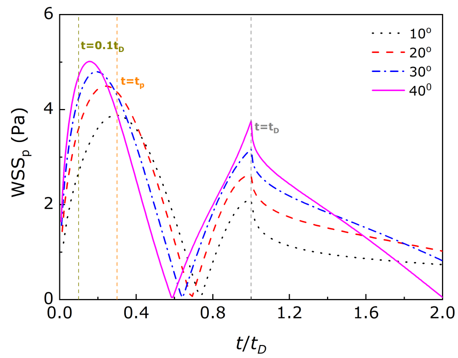

Figure 12: Wall shear stress on point P (see Fig. 1b) for saccadic amplitudes of $A = 10°$, $20°$, $30°$ and $40°$, for VH gel phase.

for a movement of $A = 40°$ is 5 Pa, while for $A = 10°$ is 3.9 Pa); the second peak occurs for $t \approx t_D$ and again larger saccades lead to higher values of WSS. For $t > t_D$ it is possible to observe that for the larger saccades the WSS in the macula region decreases faster, and interestingly for $t = 2t_D$ it is close to zero for a movement with an amplitude of $A = 40°$. That observation finding is better seen in Fig. 13, since for $t = 2t_D$ it is possible to observe considerable WSS in the centre of the lens indentation for $A = 10$, 20 and $30°$, but not for $A = 40°$. Analysing Fig. 13, it is also possible to observe that for all the tested amplitudes the maximum WSS values are reached in the centre of the lens indentation.

The $\mathrm{WSS_p}$ over time, and the WSS contours for VH liquid phase, for different amplitudes of movement, are presented in Fig. 14 and Fig. 15, respectively. For $t < t_D$, and for the different saccadic movement amplitudes, the $\mathrm{WSS_p}$ time variation follows the same trend as described for the VH gel phase. After $t = t_D$, $\mathrm{WSS_p}$ starts decreasing, but for $t = 2t_D$ the value is still not close to zero. For $t = t_p$, VH liquid phase presents higher WSS values in the region of the lens indentation but in a non-symmetrical way due to the larger inertial effects observed in this fluid (see Fig. 15).

Comparing both fluids, VH gel phase shows higher values of the average WSS

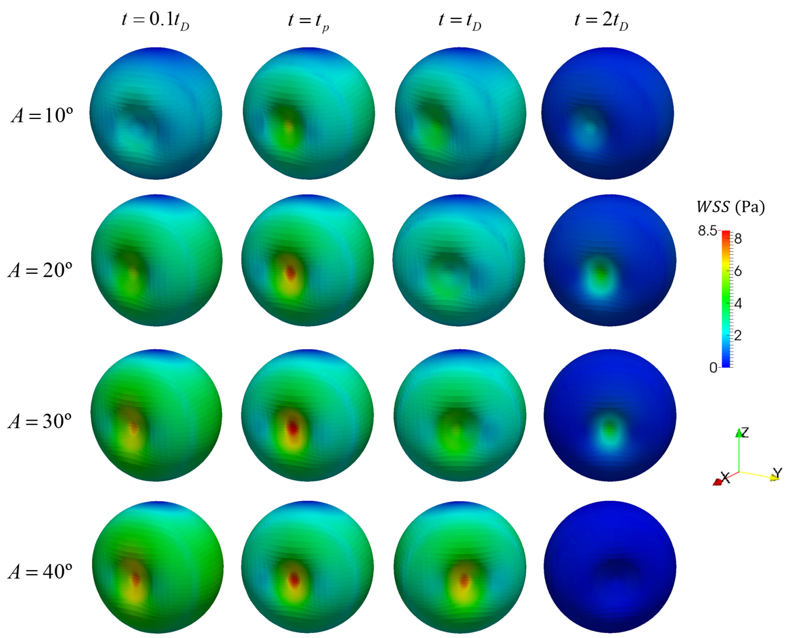

Figure 13: Wall shear stress contours on the vitreous cavity for saccadic amplitudes of $A = 10°$, $20°$, $30°$ and $40°$, at times $t = 0.1t_D$, $t = t_p$, $t = t_D$ and $t = 2t_D$, for VH gel phase.

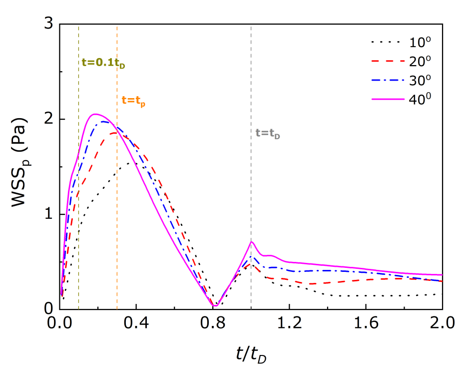

Figure 14: Wall shear stress on point P (see Fig. 1b) for saccadic amplitudes of $A = 10°$, $20°$, $30°$ and $40°$, for VH liquid phase.

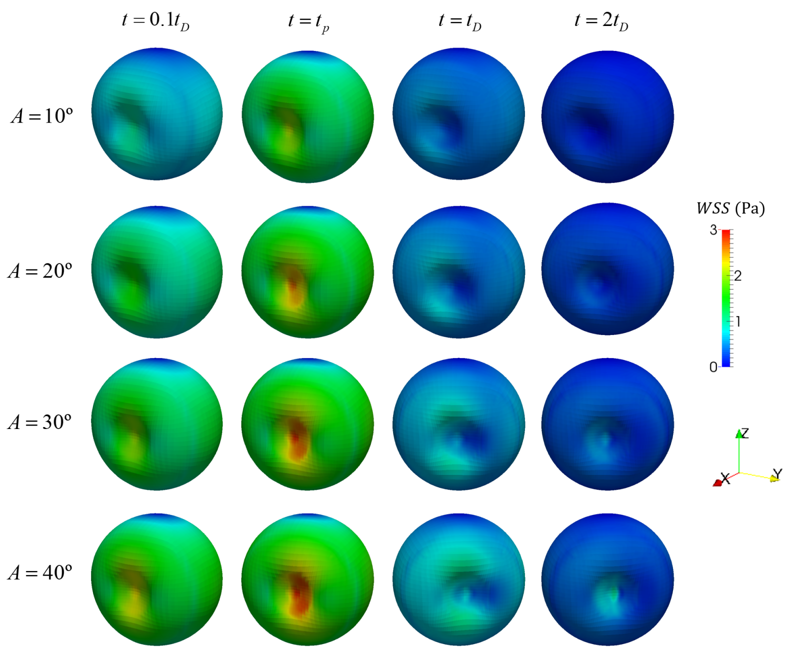

Figure 15: Wall shear stress contours on the vitreous cavity for saccadic amplitudes of $A = 10°$, $20°$, $30°$ and $40°$, at times $t = 0.1t_D$, $t = t_p$, $t = t_D$ and $t = 2t_D$, for VH liquid phase.

and the WSS at the macula region, and $\mathrm{WSS_p}$ reaches a peak between $t = 0.1t_D$ and $t = t_p$, except for the VH liquid phase when subjected to a saccade with an amplitude of $A = 10°$, where the maximum $\mathrm{WSS_p}$ occurs after $t = t_p$. For all the saccadic amplitudes tested, the maximum WSS generated by the VH gel phase are always more than twice the ones generated with the VH liquid phase (see Fig. 13 and Fig. 15): in the centre of the lens indentation and for a movement with $A = 40°$, the VH liquid gel phase reaches a maximum WSS value of approximately 8.5 Pa, while the VH liquid phases reaches 3 Pa.

In a previous work [9] we showed that VH phases present significant elastic properties, with the gel phase presenting a stronger elastic behaviour than the liquid phase. It is believed that the properties of the VH gel phase are the closest representation to those of the VH in its natural environment. This work shows that the rheological differences between VH liquid and gel phase produce significant differences in the flow behaviour of the fluids. Based on Repetto *et al.* [12], medical literature suggests that retinal detachment (RD) occurrence and progression is related to a mechanical phenomena. The stresses generated between the fluid and the retina are key to keep the retina in its proper position. The decrease of the elastic properties with the liquefaction process of the VH can contribute for the appearance of diseases as retinal detachment (RD), retinal tears (RT) and macula degeneration [46, 47]. The VH liquid phase shows WSS values much lower than VH gel phase, which may explain the increase of cases of RD and RT with VH liquefaction.

4. Conclusions

The main goal of the present work was to characterise the flow behaviour of the VH gel and liquid phases for different amplitudes of saccadic eye movements, taking into account their viscoelastic character and considering realistic eye chamber geometry and saccade profiles. To the best of our knowledge, this work is the first numerical study that simulates the liquefied VH as a viscoelastic fluid. Furthermore, the study aims to quantify the differences in the flow behaviour between VH liquid and gel phases for different amplitudes of saccadic eye movements. We used numerical simulations with complex rheological models that properly reproduce the viscoelastic VH gel and liquid behaviour measured experimentally [9].

The elasticity and the viscosity of the VH liquid phase are lower than those of the gel phase and consequently the numerical results show distinct flow behaviour. The most important differences are the fact that inertial effects are more relevant for the VH liquid phase and the $\mathrm{WSS_p}$ produced by the VH gel phase is more than the double of the values generated by VH liquid phase: for a saccadic movement with an amplitude $A = 40°$, the VH gel phase can reach $\mathrm{WSS_p}$ of 5 Pa, while the maximum $\mathrm{WSS_p}$ obtained for the VH liquid phase was 2.1 Pa. This difference may play an important role in understanding RD pathologies and macula degeneration, and proposing new therapeutics.

This work provides new insights on the flow behaviour of the different phases of VH. Here we consider that the vitreous cavity is filled with the liquid phase or with the gel phase on its own. However, during liquefaction of VH, both phases coexist inside the vitreous cavity. Further work using multiphase solvers would give new information on how both phases interact during saccadic eye movements.

Acknowledgements: A.F. Silva gratefully acknowledges the financial support from the Fundação para a Ciência e a Tecnologia (FCT) through scholarship SFRH/BD/91147/2012. Part of the results were obtained using the EPSRC funded ARCHIE-WeSt High Performance Computer (www.archiewest.ac.uk).

References

[1] J. D. Enderle, Models of Horizontal Eye Movements: Early models of saccades and smooth pursuit, no. pt. 1 in Synthesis lectures on biomedical engineering, Morgan & Claypool, 2010.
URL https://books.google.co.uk/books?id=8xyQBpT59AoC

[2] V. Kumari, E. Antonova, B. Wright, A. Hamid, E. M. Hernandez, A. Schmechtig, U. Ettinger, The mindful eye: Smooth pursuit and saccadic eye movements in meditators and non-meditators, Consciousness and Cognition 48 (2017) 66 – 75. doi:http://dx.doi.org/10.1016/j.concog.2016.10.008.
URL http://www.sciencedirect.com/science/article/pii/S1053810016302100

[3] J. Bronzino, Biomedical Engineering Handbook 2, The electrical engineering handbook series, Springer Berlin Heidelberg, 2000.
URL https://books.google.co.uk/books?id=T2UIoAxcFdIC

[4] S. Liversedge, I. Gilchrist, S. Everling, The Oxford Handbook of Eye Movements, Oxford Library of Psychology, OUP Oxford, 2011.
URL https://books.google.co.uk/books?id=Hiof9gzHPNoC

[5] T. V. Chirila, Y. Hong, P. D. Dalton, I. J. Constable, M. F. Refojo, The use of hydrophilic polymers as artificial vitreous, Progress in Polymer Science 23 (3) (1998) 475–508. doi:http://dx.doi.org/10.1016/S0079-6700(97)00045-2.
URL http://www.sciencedirect.com/science/article/pii/S0079670097000452

[6] C. S. Nickerson, H. L. Karageozian, J. Park, J. A. Kornfield, Internal tension: A novel hypothesis concerning the mechanical properties of the vitreous humor, Macromolecular Symposia 227 (1) (2005) 183–190. doi:10.1002/masy.200550918.
URL http://dx.doi.org/10.1002/masy.200550918

[7] C. S. Nickerson, J. Park, J. A. Kornfield, H. Karageozian, Rheological properties of the vitreous and the role of hyaluronic acid, Journal of Biomechanics 41 (9) (2008) 1840–1846. doi:http://dx.doi.org/10.1016/j.jbiomech.2008.04.015.
URL http://www.sciencedirect.com/science/article/pii/S0021929008001917

[8] P. Sharif-Kashani, J. P. Hubschman, D. Sassoon, H. P. Kavehpour, Rheology of the vitreous gel: effects of macromolecule organization on the viscoelastic properties, Journal of Biomechanics 44 (3) (2011) 419–23. doi:10.1016/j.jbiomech.2010.10.002.

[9] A. F. Silva, M. A. A. Alves, M. S. N. OAlves, Rheological behaviour of vitreous humour, Rheologica Acta (2017) 1–10doi:10.1007/s00397-017-0997-0.
URL http://dx.doi.org/10.1007/s00397-017-0997-0

[10] J. Black, G. W. Hastings, Handbook of Biomaterial Properties, Chapman & Hall, 1998.
URL http://books.google.pt/books?id=A9swPCp4--wC

[11] F. Baino, Towards an ideal biomaterial for vitreous replacement: Historical overview and future trends, Acta Biomaterialia 7 (3) (2011) 921–935. doi:http://dx.doi.org/10.1016/j.actbio.2010.10.030.
URL http://www.sciencedirect.com/science/article/pii/S1742706110005052

[12] R. Repetto, An analytical model of the dynamics of the liquefied vitreous induced by saccadic eye movements, Meccanica 41 (1) (2006) 101–117. doi:10.1007/s11012-005-0782-5.
URL http://dx.doi.org/10.1007/s11012-005-0782-5

[13] A. Stocchino, R. Repetto, C. Cafferata, Eye rotation induced dynamics of a newtonian fluid within the vitreous cavity: the effect of the chamber shape, Physics in Medicine & Biology 52 (7) (2007) 2021–34. doi:10.1088/0031-9155/52/7/016.

[14] T. David, S. Smye, T. Dabbs, T. James, A model for the fluid motion of vitreous humour of the human eye during saccadic movement, Physics in Medicine and Biology 43 (6) (1998) 1385.
URL http://stacks.iop.org/0031-9155/43/i=6/a=001

[15] R. Repetto, A. Stocchino, C. Cafferata, Experimental investigation of vitreous humour motion within a human eye model, Physics in Medicine and Biology 50 (19) (2005) 4729.
URL http://stacks.iop.org/0031-9155/50/i=19/a=021

[16] R. Repetto, J. H. Siggers, A. Stocchino, Mathematical model of flow in the vitreous humor induced by saccadic eye rotations: effect of geometry, Biomechanics and Modeling in Mechanobiology 9 (1) (2010) 65–76. doi:10.1007/s10237-009-0159-0.
URL http://dx.doi.org/10.1007/s10237-009-0159-0

[17] A. Stocchino, R. Repetto, J. H. Siggers, Mixing processes in the vitreous chamber induced by eye rotations, Physics in Medicine & Biology 55 (2) (2010) 453–67. doi:10.1088/0031-9155/55/2/008.

[18] O. Abouali, A. Modareszadeh, A. Ghaffariyeh, J. Tu, Numerical simulation of the fluid dynamics in vitreous cavity due to saccadic eye movement, Medical Engineering and Physics 34 (6) (2012) 681–92. doi:10.1016/j.medengphy.2011.09.011.

[19] R. Repetto, A. Tatone, A. Testa, E. Colangeli, Traction on the retina induced by saccadic eye movements in the presence of posterior vitreous detachment, Biomechanics and Modeling in Mechanobiology 10 (2) (2011) 191–202. doi:10.1007/s10237-010-0226-6.
URL http://dx.doi.org/10.1007/s10237-010-0226-6

[20] J. Meskauskas, R. Repetto, J. H. Siggers, Oscillatory motion of a viscoelastic fluid within a spherical cavity, Journal of Fluid Mechanics 685 (2011) 1–22. doi:doi:10.1017/jfm.2011.263.
URL http://dx.doi.org/10.1017/jfm.2011.263

[21] K. Isakova, J. O. Pralits, R. Repetto, M. R. Romano, Mechanical models of the dynamics of vitreous substitutes, BioMed Research International 2014 (2014) 10. doi:10.1155/2014/672926.
URL http://dx.doi.org/10.1155/2014/672926

[22] A. Bonfiglio, A. Lagazzo, R. Repetto, A. Stocchino, An experimental model of vitreous motion induced by eye rotations, Eye and Vision 2 (1) (2015) 1–10. doi:10.1186/s40662-015-0020-8.
URL http://dx.doi.org/10.1186/s40662-015-0020-8

[23] A. Modarreszadeh, O. Abouali, Numerical simulation for unsteady motions of the human vitreous humor as a viscoelastic substance in linear and non-linear regimes, Journal of Non-Newtonian Fluid Mechanics 204 (2014) 22–31. doi:http://dx.doi.org/10.1016/j.jnnfm.2013.12.001.

URL http://www.sciencedirect.com/science/article/pii/S0377025713002036

[24] J. L. Favero, A. Secchi, N. Cardozo, H. Jasak, Viscoelastic flow simulation: Development of a methodology of analysis using the software openfoam and differential constitutive equations, Computer Aided Chemical Engineering 27 (2009) 915 – 920, 10th International Symposium on Process Systems Engineering: Part A. doi:http://dx.doi.org/10.1016/S1570-7946(09)70373-6.
URL http://www.sciencedirect.com/science/article/pii/S1570794609703736

[25] R. K. Balachandran, V. H. Barocas, Contribution of saccadic motion to intravitreal drug transport: Theoretical analysis, Pharmaceutical Research 28 (5) (2011) 1049–1064. doi:10.1007/s11095-010-0356-7.
URL http://dx.doi.org/10.1007/s11095-010-0356-7

[26] K. E. Swindle, P. D. Hamilton, N. Ravi, In situ formation of hydrogels as vitreous substitutes: Viscoelastic comparison to porcine vitreous, Journal of Biomedical Materials Research Part A 87A (3) (2008) 656–665. doi:10.1002/jbm.a.31769.
URL <GotoISI>://WOS:000260984800011

[27] B. Lee, Comparative rheological studies of the vitreous body of the eye, Dissertations available from ProQuest. Paper AAI9227704. http://repository.upenn.edu/dissertations/AAI9227704.

[28] J. Meskauskas, R. Repetto, J. H. Siggers, Shape change of the vitreous chamber influences retinal detachment and reattachment processes: Is mechanical stress during eye rotations a factor?vitreous stress on the retina, Investigative Ophthalmology & Visual Science 53 (10) (2012) 6271–6281. doi:10.1167/iovs.11-9390.
URL http://dx.doi.org/10.1167/iovs.11-9390

[29] D. Natali, R. Repetto, J. H. Tweedy, T. H. Williamson, J. O. Pralits, A simple mathematical model of rhegmatogenous retinal detachment, Journal of Fluids and Structures 82 (2018) 245 – 257. doi:https://doi.org/10.1016/j.jfluidstructs.2018.06.020.
URL http://www.sciencedirect.com/science/article/pii/S0889974617308800

[30] E. Y. K. Ng, J. H. Tan, U. R. Acharya, J. S. Suri, Human Eye Imaging and Modeling, CRC Press, 2012.
URL https://books.google.co.uk/books?id=mPrRBQAAQBAJ

[31] E. S. Perkins, H. Davson, Human eye, Encyclopaedia Britannica, inc. (June 2018).
URL https://www.britannica.com/science/human-eye

[32] W. Becker, The neurobiology of saccadic eye movements. Metrics, PHI Learning, 2006.
URL https://books.google.co.uk/books?id=KEzdXmXgaHkC

[33] E. M. del Amo, A. Urtti, Rabbit as an animal model for intravitreal pharmacokinetics: Clinical predictability and quality of the published data, Experimental Eye Research 137 (2015) 111–124. doi:http://dx.doi.org/10.1016/j.exer.2015.05.003.
URL http://www.sciencedirect.com/science/article/pii/S0014483515001451

[34] T. T. Kleinberg, R. T. Tzekov, L. Stein, N. Ravi, S. Kaushal, Vitreous substitutes: A comprehensive review, Survey of Ophthalmology 56 (4) (2011) 300–323. doi:http://dx.doi.org/10.1016/j.survophthal.2010.09.001.
URL http://www.sciencedirect.com/science/article/pii/S003962571000161X

[35] H. Giesekus, A simple constitutive equation for polymer fluids based on the concept of deformation-dependent tensorial mobility, Journal of Non-Newtonian Fluid Mechanics 11 (12) (1982) 69 – 109.

doi:http://dx.doi.org/10.1016/0377-0257(82)85016-7. URL http://www.sciencedirect.com/science/article/pii/0377025782850167

[36] M. Pflaumbaum, H. Rehage, Myristyl dimethylamine oxide surfactant solutions: Model systems for rheological research, ChemPhysChem 4 (7) (2003) 705–713. doi:10.1002/cphc.200200585. URL http://dx.doi.org/10.1002/cphc.200200585

[37] S. Kheirandish, I. Gubaydullin, N. Willenbacher, Shear and elongational flow behavior of acrylic thickener solutions. part ii: effect of gel content, Rheologica Acta 48 (4) (2009) 397–407. doi:10.1007/s00397-008-0324-x. URL http://dx.doi.org/10.1007/s00397-008-0324-x

[38] M. Keshavarz, B. Kaffashi, The ability of retention, drug release and rheological properties of nanogel bioadhesives based on cellulose derivatives, Pharmaceutical Development and Technology 19 (8) (2014) 952–959. arXiv:http://dx.doi.org/10.3109/10837450.2013.846371, doi:10.3109/10837450.2013.846371. URL http://dx.doi.org/10.3109/10837450.2013.846371

[39] P. A. Vasquez, Y. Jin, E. Palmer, D. Hill, M. G. Forest, Modeling and simulation of mucus flow in human bronchial epithelial cell cultures - part i: Idealized axisymmetric swirling flow, PLoS Computational Biology 12. doi:10.1371/journal.pcbi.1004872. URL http://adsabs.harvard.edu/abs/2016PLSCB..12E4872V

[40] J. Azaiez, R. Gunette, A. At-Kadi, Numerical simulation of viscoelastic flows through a planar contraction, Journal of Non-Newtonian Fluid Mechanics 62 (2) (1996) 253 – 277. doi:https://doi.org/10.1016/0377-0257(95)01406-3. URL http://www.sciencedirect.com/science/article/pii/0377025795014063

[41] F. A. Morrison, Understanding Rheology, Oxford University Press, 2001.
URL https://books.google.co.uk/books?id=bwTn8ZbR0C4C

[42] M. A. Alves, P. J. Oliveira, F. T. Pinho, A convergent and universally bounded interpolation scheme for the treatment of advection, International Journal for Numerical Methods in Fluids 41 (1) (2003) 47–75. doi:10.1002/fld.428.
URL http://dx.doi.org/10.1002/fld.428

[43] R. Fattal, R. Kupferman, Time-dependent simulation of viscoelastic flows at high weissenberg number using the log-conformation representation, Journal of Non-Newtonian Fluid Mechanics 126 (1) (2005) 23 – 37. doi:https://doi.org/10.1016/j.jnnfm.2004.12.003.
URL http://www.sciencedirect.com/science/article/pii/S0377025705000042

[44] A. Afonso, P. Oliveira, F. Pinho, M. Alves, The log-conformation tensor approach in the finite-volume method framework, Journal of Non-Newtonian Fluid Mechanics 157 (12) (2009) 5565.
URL http://www.sciencedirect.com/science/article/pii/S0377025708001730

[45] F. Pimenta, M. A. Alves, Stabilization of an open-source finite-volume solver for viscoelastic fluid flows, Journal of Non-Newtonian Fluid Mechanics 239 (2017) 85 – 104. doi:http://dx.doi.org/10.1016/j.jnnfm.2016.12.002.
URL http://www.sciencedirect.com/science/article/pii/S0377025716303329

[46] M. M. Le Goff, P. N. Bishop, Adult vitreous structure and postnatal changes, Eye 22 (10) (2008) 1214–1222.
URL http://dx.doi.org/10.1038/eye.2008.21

[47] J. Sebag, S. Nie, K. Reiser, M. A. Charles, N. T. Yu, Raman spectroscopy

of human vitreous in proliferative diabetic retinopathy, Investigative Ophthalmology & Visual Science 35 (7) (1994) 2976–80.